Analysis of End-Stop Oscillations in an AsymmetricHydraulic Steering Unit

Pedersen, Mathias G. ; Amstrup, Sanne; Olesen, Emil Nørregård; Andersen, Torben Ole; Pedersen, Henrik C.

Published in:
Proceedings The 18th Scandinavian International Conference on Fluid Power, SICFP'23

Publication date:
2023

Document Version
Accepted author manuscript, peer reviewed version

The 18th Scandinavian International Conference on Fluid Power, SICFP'23, May 30- June 1, 2023, Tampere, Finland

Analysis of End-Stop Oscillations in an Asymmetric Hydraulic Steering Unit

M.G. Pedersen[1], S. Amstrup[2], E.N. Olesen[1], T.O. Andersen[3], and H.C. Pedersen[3]

[1]Danfoss Power Solutions, Nordborg, Denmark
[2]Liftra, Aalborg, Denmark
[3]Department of Energy, Aalborg University, Aalborg, Denmark
E-mail: mathias.pedersen@danfoss.com, sam@liftra.dk, emil.olesen@danfoss.com, toa@energy.aau.dk, hcp@energy.aau.dk

Abstract

Danfoss Power Solutions ApS (DPS) has a product line of hydrostatic steering units for heavy-duty machines. The focus of this paper is on oscillations occurring in an asymmetrical hydraulic steering unit called sSteering. This concept, which is hydraulic asymmetric, increases the steering responsiveness between the steering wheel input and the output. One of the challenges with this asymmetry refers to the end-stop situation. This challenge is related to the left end-stroke of the cylinder, where the concept suffers from a relatively low end-stop torque, that indicates to the operator that the maximum turning angle is reached. Different solutions to increase this torque have been investigated, but each with the drawback of introducing underdamped oscillations of the steering wheel. The objective of the current paper is thus to investigate the concept and identify the root cause for the underdamped response.
The end-stop situation is analyzed through a lumped-parameter model, which is able to imitate the dynamics causing the oscillations. The oscillations seen in the model, are found to be present when the torque input is in a limited range. Through analysis of the model responses, the root cause is found to be a chain of events, which is initiated by the opening of a hydraulic bleed row in the end-stop situation. This bleed row has an impact on the torque balance of the steering unit's internal components, which initiates the underdamped oscillations of the steering wheel. Finally, a sensitivity analysis is conducted, to clarify which model parameters that have a crucial impact on the oscillations, and to understand how these oscillations may be dampened.

Keywords: Rotary spool/sleeve valve, Underdamped oscillations, asymmetric hydraulic steering unit

1 Introduction

Hydraulic power steering is of interest in a wide range of heavy-duty agricultural and material-handling vehicles, where an Orbital Steering Pump (OSP) is an easy and flexible solution for closed loop control of the steering system. Crucial elements for steering systems in such vehicles are operator safety and comfort. In recent years, speed limit regulations have been increased up to 65 km/h in various European countries [1]. This trend increases the mental workload of the operator during steering according to [2] [3], it is therefore of interest to improve the ease of steering. Operability of the heavy vehicle during road driving relies on the interplay between steering input from the operator and the steering system and is therefore highly dependent on the ability to transfer the desired trajectory of the wheels (output) through the steering wheel (input) [4].

State-of-the-art solutions regarding hydraulic power steering consist of hydrostatic and electrohydraulic solutions. State-of-the-art hydrostatic solutions are described in the catalog [5], where the solution depends on the given application. Various solutions exist, where key parameters for the operator is the torque felt by the operator, and the dead band of the closed loop system. A typical dead-band within these units is $\pm 2^{o}$, which is present in between the input and output of the steering system. State-of-the-art electrohydraulic solutions are based on steer-by-wire force feedback systems [6], where the operator is controlling the input to the steering system through an input

device. This device is often a joystick or mini wheel, which is electrically connected to an electrohydraulic valve. A typical dead-band for such a unit can be controlled depending on the software, but according to [7] the dead-band is optimal in the range of $\pm 4 - 6^{o}$.

In a recent study, a new hydrostatic steering concept is investigated, which eliminates the dead band between operator input and output [8]. This concept is hydraulic asymmetric, which thereby enables the possibility to design the hydraulic valve characteristics as being under-lapping. The under-lapping design results in a pressure balanced steering unit that eliminates the state-of-the-art dead band. According to the paper, [9] this concept reduces the mental workload for the operator during driving and indicates that the concept is easier to operate compared to a state-of-the-art steering system. The drawback of this new concept is the asymmetry in the hydraulic system, which introduces challenges compared to present units. One of these problems concerns the end-stop torque, when an end-stroke of the cylinder/wheel position is reached, in which case the operator doesn't feel an end-stop torque at the left end-stroke, in the steering wheel. To address this issue different attempts have been made, but these tempt to introduce underdamped oscillations in the steering wheel when reaching the left end-stroke and cause an unpleasant driving experience for the operator.

As the end stop feeling is a crucial parameter for a steering system, it is therefore of interest to understand the root cause of these responses. Therefore, the objective of this paper will be to model the existing solutions and analyze the model, to be able to describe the root cause of the underdamped oscillation response. The paper is organized as follows:

Section two describes the functionality of an asymmetric steering unit, and a lumped parameter model is presented in section three. The model is verified in section four which constitutes the foundation for an analysis and sensitivity study of the model in section five. Finally, section six concludes with the findings of the paper.

2 System Description

To understand the design and behavior of a steering unit, figs. 1 and 2 are used as references. Figure 1 illustrates an exploded view of the steering unit with its components and fig. 2 illustrates the working principle for a left turn of the unit and thereby vehicle.

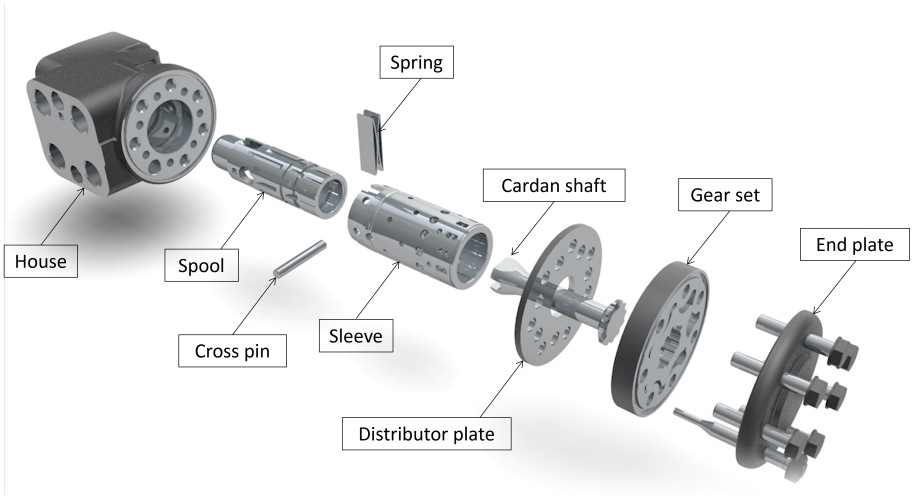

Figure 1: This illustrates the exploded view of the components contained in the steering unit.

The steering unit functions by metering out hydraulic fluid for either the left or right cylinder chamber. When the operator applies an input on the steering wheel, the spool rotates continuously with the input from the operator which compresses the spring package between the spool and sleeve that results in a relative angle, α. This causes holes in the sleeve to align with groves in the spool allowing hydraulic fluid to flow through the steering unit.

The flow path is asymmetric, such that when steering right the flow is going through the spool and sleeve and then metered through the gear set to the cylinder where the returning oil is led to the tank through the spool and sleeve. When steering left the oil is directly flowing to the cylinder, and it is instead the returning flow that is metered to the tank. This asymmetry in the architecture enables the possibility to design the spool and sleeve as an under-lapping valve system which eliminates the dead band because the cylinder at all times is controlled through a pressure balancing valve system where a small deviation of the relative angle will cause a pressure change for either left or right cylinder port. To ensure the system can create the pressure balancing of the cylinder ports, the asymmetric

design must have a small flow at all times, where the flow will be balanced between the port connection and tank connection. In this paper, a prototype for a Dynamic Load Sensing unit is considered, where the LS line delivers a small amount of flow. An overview of the internal flow path is shown in the figure2.

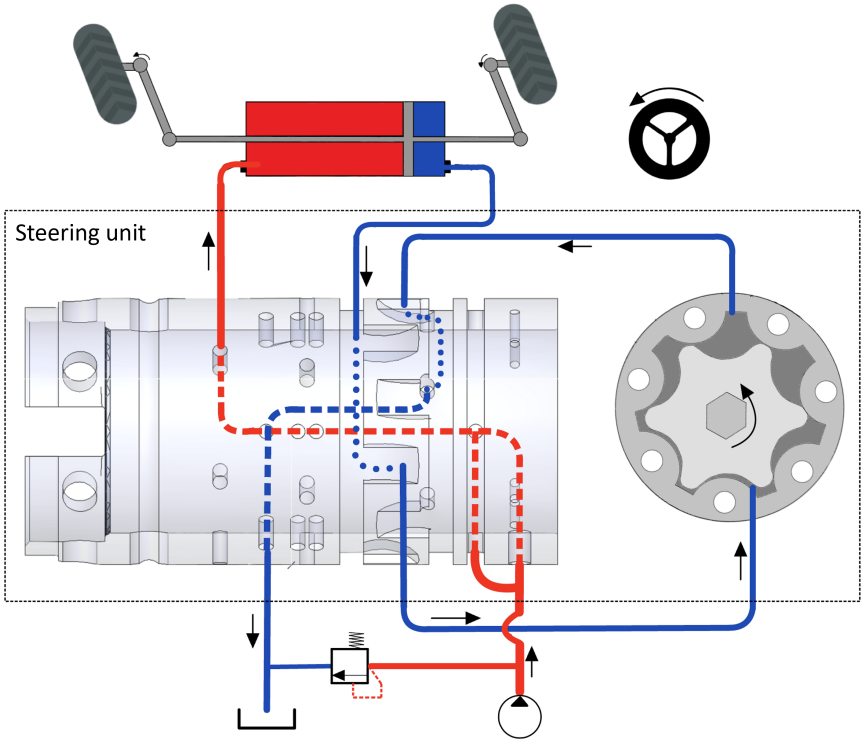

Figure 2: Illustrated is the flow pattern in the hydrostatic steering circuit during a left turn. Red illustrates the high-pressure side, blue is the low-pressure side and the dotted line is the flow paths in the sleeve and the stippled line is inside the spool. Curved direction arrows define the direction of the rotation and straight arrow defines the flow direction.

3 Lumped-parameter model

To analyze the behavior, a lumped-parameter model is derived for a simplified system of the hydrostatic steering circuit, as seen in fig. 4 and described in the following.

3.1 Hydraulic model

The hydraulic model describes the flows Q_i and pressures p_i in the hydrostatic steering circuit. The flow through the orifices with the corresponding area A_i and discharge coefficient C_d are dependent on the relative angle between the spool and sleeve, where the area increases with an increase in relative angle, α. The α dependent flows are modelled based on the orifice equation where the hydraulic fluid is assumed to have a constant viscosity of ρ:

$$Q_i = C_d A_i(\alpha)(\sqrt{\frac{2}{\rho}|(\Delta P)|}\,\mathrm{sgn}(\Delta P) \tag{1}$$

Where i refers to the respective orifices marked with red in 4. The flow through the gear set is dependent on the velocity of the sleeve, $\dot{\theta}_{SL}$ and its given displacement D_{GS}, where the leakage is assumed laminar and dependent on the leakage coefficient, C_{le} and the pressure difference on each side of the gear set:

$$Q_{GS} = D_{GS}\,\dot{\theta}_{SL} + C_{le}\,(P_{2R} - P_R) \tag{2}$$

The check valves FL and FR are modelled by a second-order polynomial and fitted to a P-Q curve. Therefore, the flows in eq. (3) and (4) are equal to zero, when the pressures P_R and P_L are greater then P_T. The flow of the two check valves writes:

$$Q_{FR} = \begin{cases} a_1(P_T - P_R)^2 + a_2(P_T - P_R) & \text{for } P_R < P_T \\ 0 & \text{for } P_R \geq P_T \end{cases} \tag{3}$$

$$Q_{FL} = \begin{cases} a_1(P_T - P_R)^2 + a_2(P_T - P_R) & \text{for } P_L < P_T \\ 0 & \text{for } P_L \geq P_T \end{cases} \tag{4}$$

As the pressure relief valve is unidirectional, the flow is zero, when the pressure difference over the pressure relief valve is less than the cracking pressure, P_{RF}. The flow for the pressure relief valve writes:

$$Q_{RF} = \begin{cases} a_3(P_1 - P_T - P_{RF}) & \text{for } (P_1 - P_T) \geq P_{RF} \\ 0 & \text{for } (P_1 - P_T) < P_{RF} \end{cases} \tag{5}$$

Where the correction factors write a_3, Q_i are the respective flow, the respective control volumes are V_i and bulk modulus is β_{eff}. Furthermore, the positive flow directions are indicated by the arrows in fig. 4.

The pressure gradient derived for all control volumes is based on the continuity equation [10] and writes for control volume 1:

$$\dot{P}_1 = (Q_1 + Q_{LS} - Q_{2R} - Q_{2L} - Q_{1314} - Q_{RF}) \frac{\beta_{eff}}{V_1} \tag{6}$$

To determine the pressure gradient, the pressure dependent effective bulk modulus is incorporated in order to take the compressibility of air dissolved in hydraulic fluid into consideration. Where a is the amount of dissolved air in the hydraulic fluid and n is the exspandebility factor for air. This is modelled by:

$$\beta_{eff} = \frac{(1-a)\exp\left(\frac{P_0-P}{\beta_0}\right) + a\left(\frac{P_0}{P}\right)^{\frac{1}{n}}}{\frac{1-a}{\beta_0}\exp\left(\frac{P_0-P}{\beta_0}\right) + \frac{a}{nP_0}\left(\frac{P_0}{P}\right)^{\frac{n+1}{n}}} \tag{7}$$

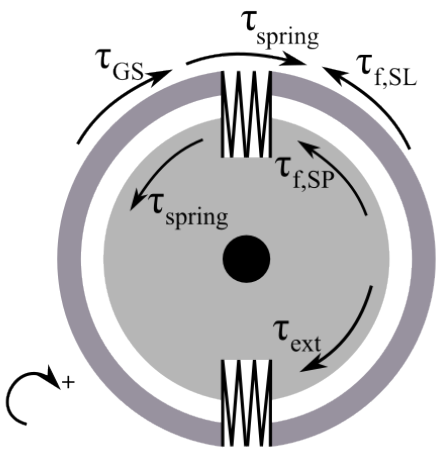

Figure 3: Illustration of the torques and reaction torques acting on the spool and sleeve.

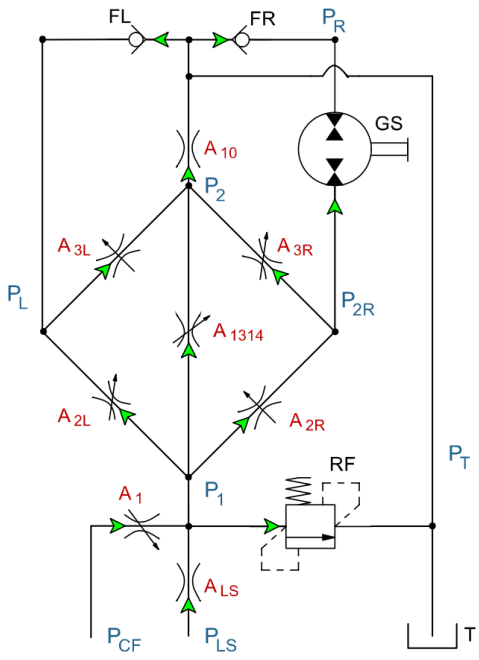

Figure 4: Diagram of the modeled system, the control volumes are marked with blue, the orifices are marked with red and the green arrows indicate the definition of positive flow through orifices utilized in the equations.

3.2 Mechanical model

The mechanical model is derived based on a mass-spring-damper system for the two rotating bodies, where their directions are illustrated in fig. 3.

By applying Newton's second law, the acceleration of the body of the spool is derived as:

$$\ddot{\theta}_{SP} = \frac{1}{J_{SP}} \cdot \Big(\tau_{ext} - \underbrace{k(\gamma)(\theta_{SP} - \theta_{SL})}_{\tau_{spring}} - \underbrace{B_{SP}(\dot{\theta}_{SP} - \dot{\theta}_{SL})}_{\tau_{f,SP}} \Big) \tag{8}$$

Here J_{SP} is the inertia of the spool, τ_{ext} is the external torque delivered by the operator, k is the spring stiffness, θ_{SP} the angle of the spool, θ_{SL} the angle of the sleeve and B_{SP} the viscous friction coefficient for the spool.

Similarly, the acceleration of the sleeve is derived as:

$$\ddot{\theta}_{SL} = \frac{1}{J_{SL}} \cdot \Big(\underbrace{k(\gamma)\,(\theta_{SP} - \theta_{SL})}_{\tau_{spring}} + \underbrace{D_{GS}(P_{2R} - P_R)}_{\tau_{GS}} - \tau_{f,SL} \Big) \tag{9}$$

Here is J_{SL} the inertia of the sleeve, cardan shaft, and gearset, $\tau_{f,SL}$ is the friction torque working against the rotation of the sleeve and gearset, τ_{spring} is the torque contribution from the spring which is found through an experimental test, where the spring motion is limited to +- 15 degrees due to a mechanical constraint in the spool.

3.3 Friction model

Friction is present for the two bodies, but the approach for describing it differs for the two. The friction is separated in two directions, the longitudinally direction and the radial direction. The friction contribution from the longitudinally direction is due to a sealing and bearing, which influence is static [11] and is neglected in this study. The contribution in the radial direction for the spool and sleeve is a lubrication film from the hydraulic oil, which is assumed to be viscous. The film will have a resistance against shear flow between the spool/sleeve and sleeve/housing surface due to the dynamic viscosity of the fluid. Figure 5 illustrates the thin oil film between spool/sleeve.

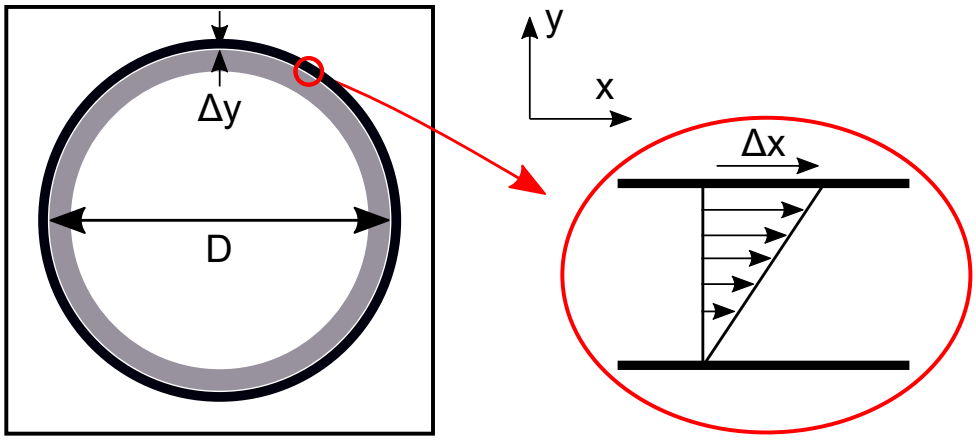

Figure 5: A illustration of the shear stress distribution between the spool and sleeve.

The spool/sleeve viscous friction is modelled with equation 10, where $\tau_{f,SP}$ is the friction torque, B_{SP} is the viscous frcition coefficient and $\dot{\theta}_i$ is the angular velocity of the spool and sleeve:

$$\tau_{f,SP} = B_{SP}(\dot{\theta}_{SP} - \dot{\theta}_{SL}) \tag{10}$$

The friction acting on the body of the sleeve includes the viscous friction between the sleeve/housing as well as the friction in the gear set. According to [12], the friction in the gear set is found to fit with the Stribeck curve, where the gear set friction is having the greatest impact on the $\dot{\theta}_{SL}$ dependent friction terms. Stribeck friction is a combination of Coulomb friction, viscous friction, and stiction and is implemented based on [13]. Furthermore a hyperbolic tangent function, tanh is inserted into the equation to prevent numerical instabilities, when $\dot{\theta}_{SL}$ is crossing zero.

Stribeck friction is only valid at $\dot{\theta}_{SL} \neq 0$. Thus, the friction acting on the body of the spool is expressed by two functions in eq. (11), which writes:

$$\tau_{f,SL} = \begin{cases} B_{SL}\dot{\theta}_{SL} + \tanh(|\dot{\theta}_{SL} \cdot 10|)\text{sgn}(\dot{\theta}_{SL})(\tau_c + |\tau_s^*|)) & \text{for } \dot{\theta}_{SL} \neq 0 \\ \tau_{aux} & \text{for } \dot{\theta}_{SL} = 0 \end{cases} \tag{11}$$

The stiction term is determined with eq. (12), this ensures that the stiction is decreasing with an increase in $\dot{\theta}_{SL}$ [13]. Equation 12 is substituted into eq. (11) and the function for Stribeck friction is expressed as:

$$|\tau_s^*| = \tau_s \exp\left(-\frac{|\dot{\theta}_{SL}|}{c_s}\right) \tag{12}$$

When $\dot{\theta}_{SL} = 0$, the upper expression in eq. (11), is not valid. Equation 13 for τ_{aux} is therefore derived as the friction for $\dot{\theta}_{SL} = 0$ and is further based on the sum of the applied torque, expressed in eq. (14). The equations expressing the friction, when $\dot{\theta}_{SL} = 0$ writes:

$$\tau_{aux} = \begin{cases} (\tau_c + \tau_s)\text{sgn}(\tau_{sum}) & \text{for } |\tau_{sum}| \geq (\tau_c + \tau_s) \\ \tau_{sum} & \text{for } |\tau_{sum}| < (\tau_c + \tau_s) \end{cases} \tag{13}$$

The sum of the remaining torques acting on the sleeve is expressed as:

$$\tau_{sum} = k(\gamma)(\theta_{SP} - \theta_{SL}) + D_{GS}(P_{2R} - P_R) \tag{14}$$

4 Verification of model

To determine the validity, the lumped parameter model responses are verified against experimental data, where the spectrum of the oscillations is examined with both the input of the experimental data, as well as a constant torque input.

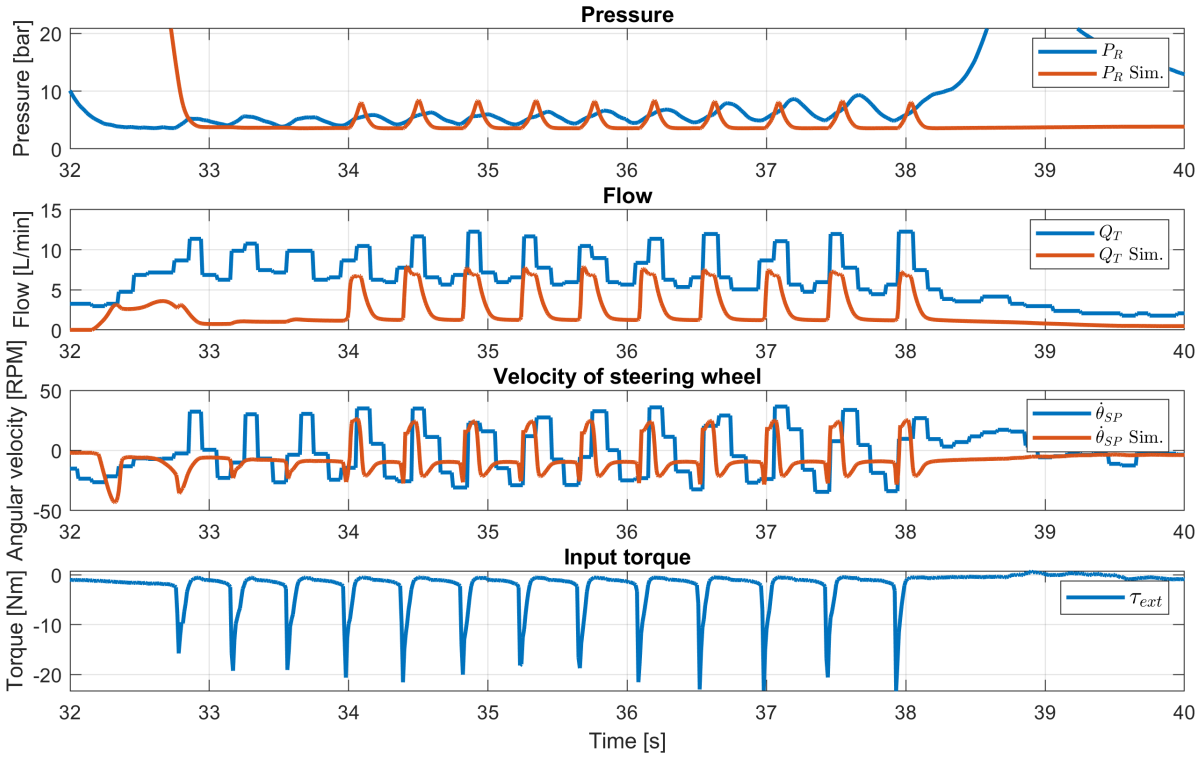

Figure 6: Comparison between model response and experimental measurements

In fig. 6 the response from the simulation model is compared with experimental lab data, conducted by DPS in Nordborg, Denmark. The pressure response, P_R, and velocity response for the steering wheel, $\dot{\theta}_{SP}$ are found to be similar. Furthermore, a comparison between the measured and simulated flow of Q_T is shown. These plots indicate that the flows have similar dynamics. However, a bias occurs between the two responses of approximately 5 L/min, where the measured flow is the highest.

The oscillating input torque, τ_{ext} in the experimental data, is illustrated in fig. 6 from 33 s to 38 s, which is also affected by the oscillations in the rest of the system. Thus, it is necessary to investigate whether the oscillations in the response from the simulation are caused by the oscillations in τ_{ext} or by the model dynamics. Between 33 s and 34 s in fig. 6, τ_{ext} is oscillating, but the simulated P_R, Q_T and $\dot{\theta}_{SP}$ are insignificantly affected. It is first when $\dot{\theta}_{SP}$ crosses zero at 34 s, that these responses are oscillating. The model is further validated with a constant torque input, as shown in fig. 7. Here, the oscillations still occur, and it can therefore be confirmed, that dynamics in the model causes the oscillations and that the model is able to represent the oscillation in P_R, Q_T and $\dot{\theta}_{SP}$. The oscillations in the model are of higher frequency in fig. 7 compared to fig. 6, this is caused by the change in input torque as the oscillations appear in the interval of -2.5 to -5 Nm for τ_{ext}, where the oscillations in the input, causes the applied torque to outside the interval of oscillations.

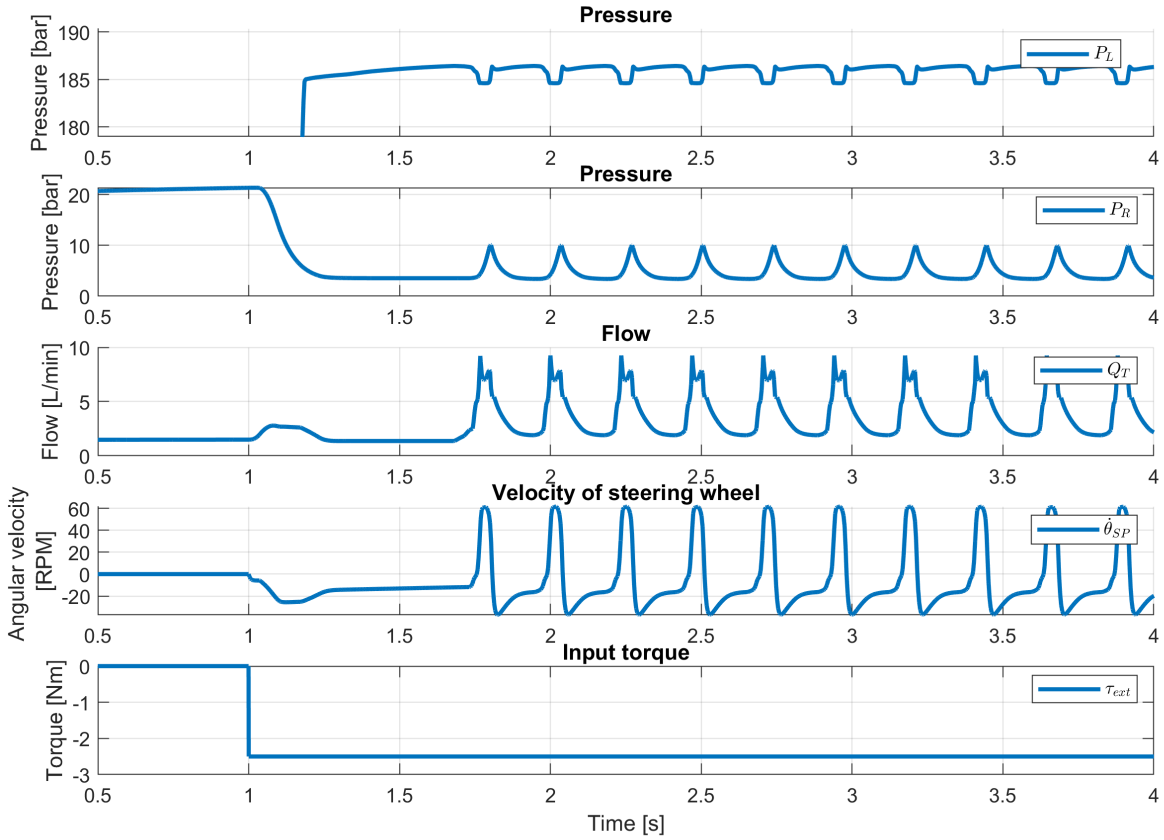

Figure 7: Model response for a step input

5 Analysis

To determine the root cause of the underdamped oscillations the model responses are analyzed in the following. This is conducted through a sensitivity analysis to clarify which parameters have a reducing effect on the oscillations.

5.1 Comparative Analysis

The state of the system varies depending on the steering direction. Observations from experimental data indicate, that the underdamped response only occurs in the left end stop when the orifices A_{1314} is included. This is also

seen in fig. 8, which shows the main pressures and flows, for respectively a left and right end-stop situation.

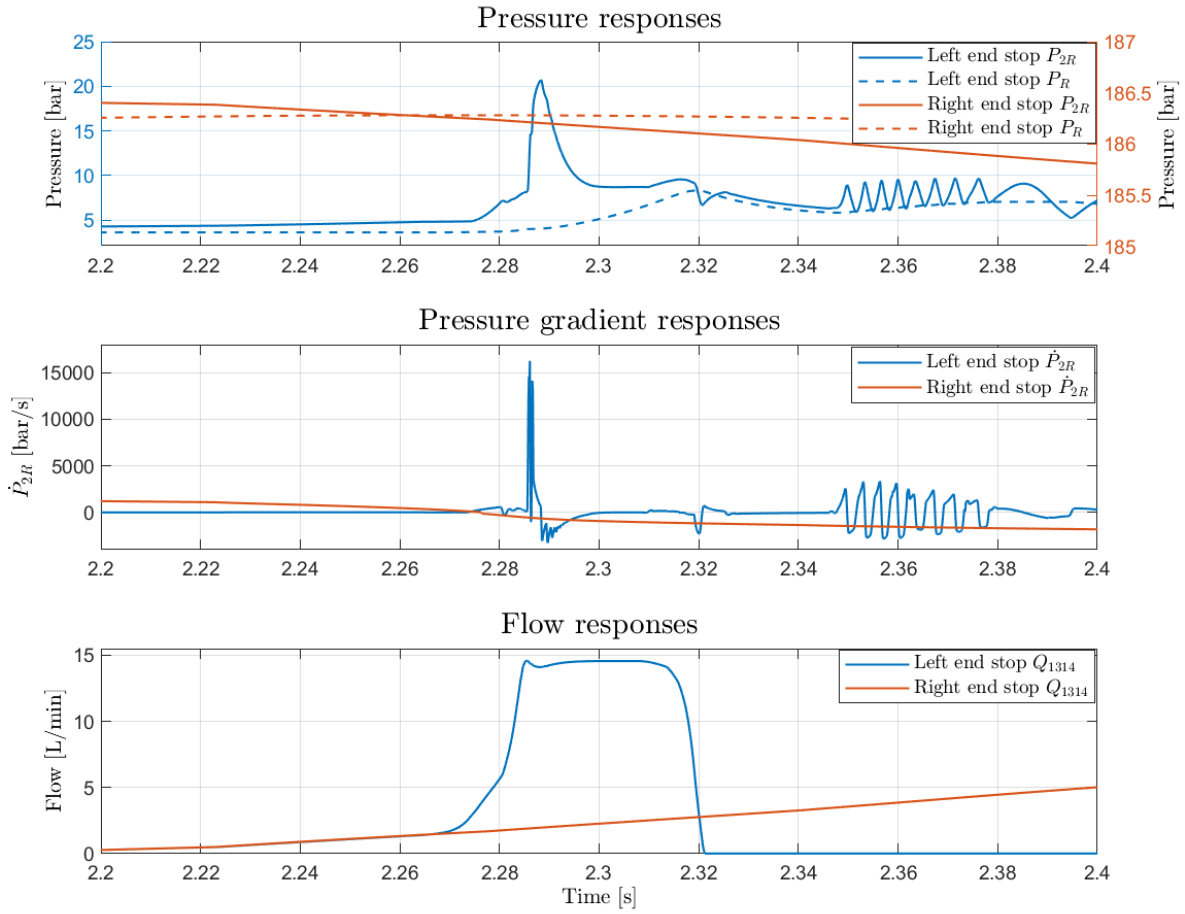

Figure 8: The responses for left and right end-stop situations when A_{1314} opens for a single oscillation.

To describe this behavior fig. 9 illustrates the states prior to the opening of A_{1314} which opens for a relative angle between spool and sleeve, $\alpha = 13°$. The prevalence of A_{10} and the opening of A_{1314} causes the pressure in the control volumes, P_2, and thereby also P_{2R} to increase. Whereas, the pressure in P_{2R} in the right end stop is insignificantly affected by the opening of A_{1314}.

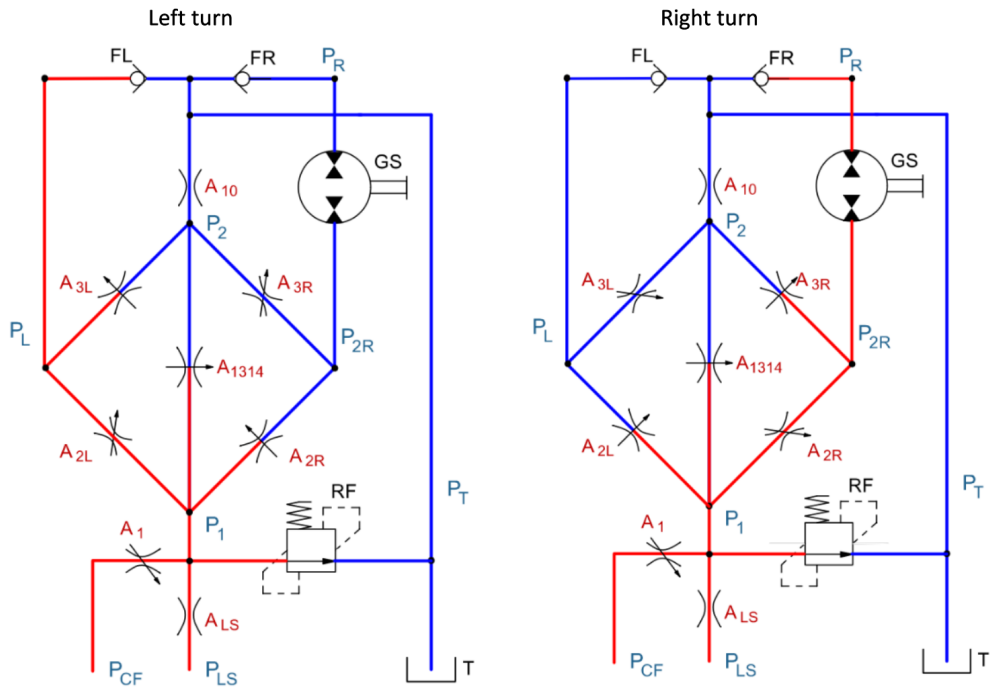

Figure 9: Hydraulic diagram for a left and a right turn before A_{1314} opens, with red representing the high-pressure side connected to the pump and blue the low-pressure side connected to the tank.

The responses with and without A_{1314} are conducted with a torque applied as a ramp input of -1 Nm/s. The oscillations are found to only occur with the prevalence of A_{1314} as illustrated in fig. 10. The responses for the angular velocity of the spool, $\dot{\theta}_{SP}$ shows that $\dot{\theta}_{SP} \neq 0$ without A_{1314}. This entails that the steering wheel is rotating and thereby no end-stop feeling is present.

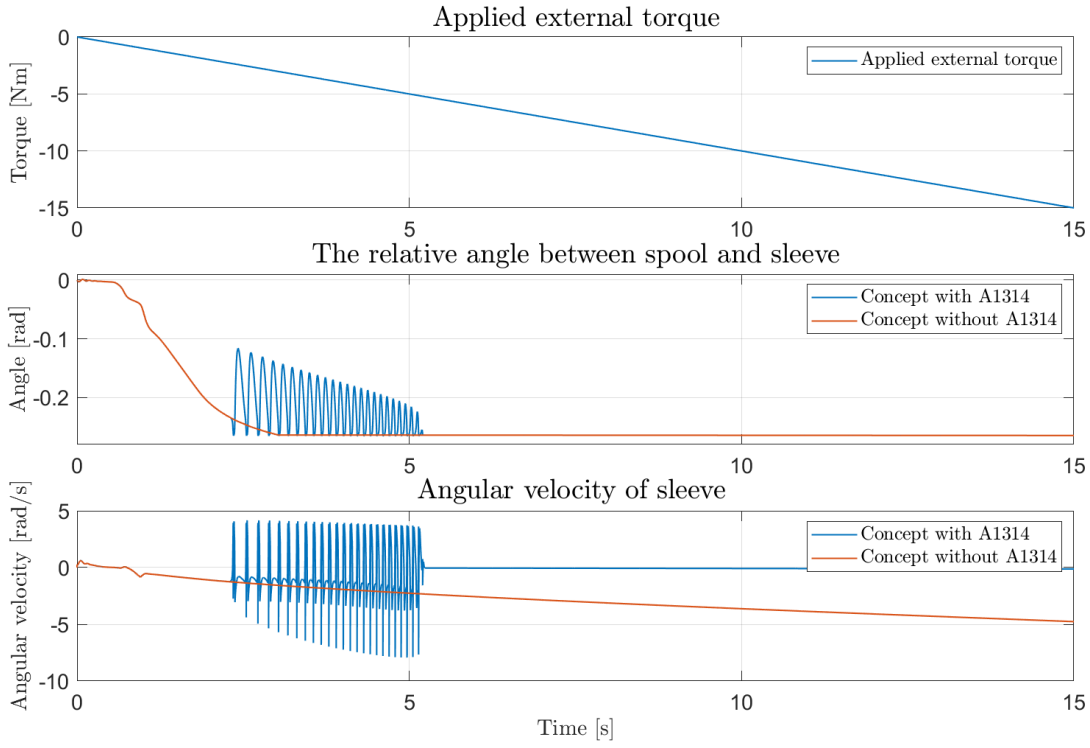

Figure 10: Comparison between the responses of the model with and without A_{1314}.

5.2 Oscillation Study

To understand the occurring behavior, one may consider eq. 9 and the state of the system before the opening A_{1314}. It is found, that the opening of A_{1314} causes a pressure increase in P_{2R}, by which the gear set torque increases and thereby further increases the acceleration in the sleeve. As fig. 11 indicates, the torques acting on the sleeve are relatively high during oscillations compared to prior to and afterward the oscillations.

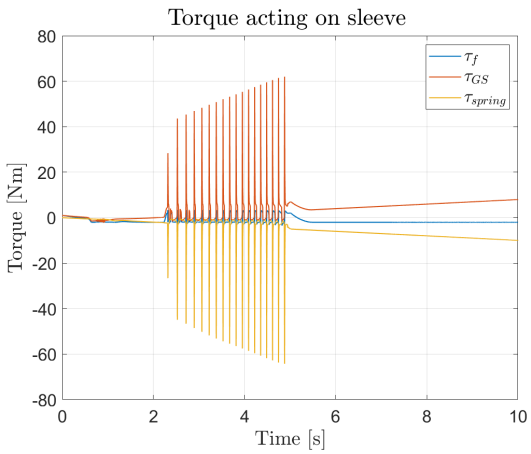

Figure 11: Simulated oscillation of the reaction torque acting on the sleeve

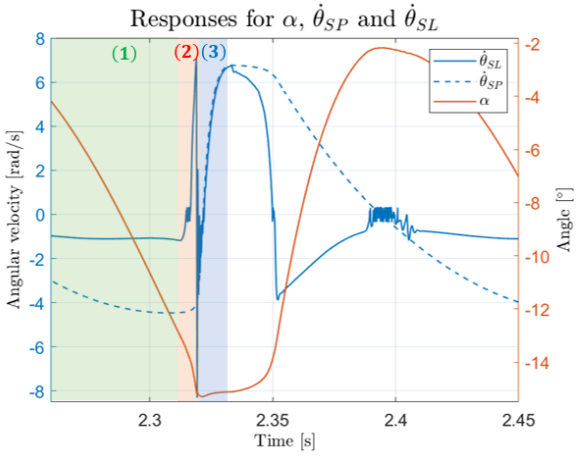

Figure 12: Simulated states during one oscillation.

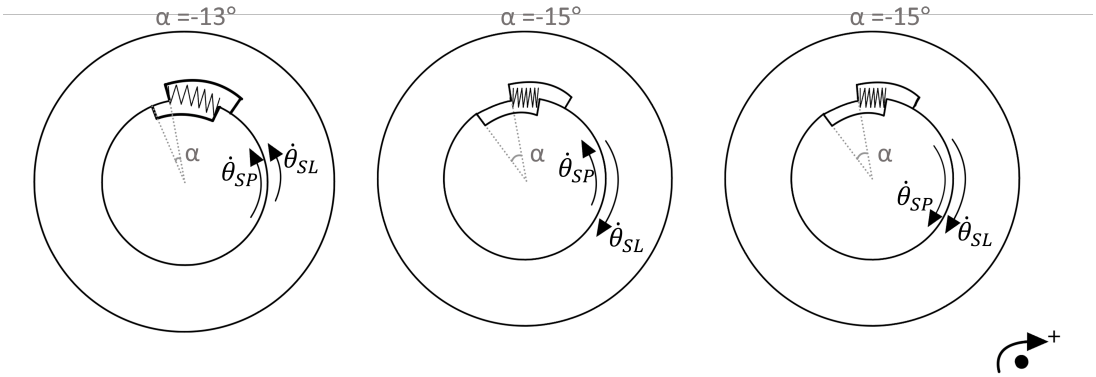

Figure 13: Illustrated are the two bodies in three instances surrounding the impact situation. The curved arrow illustrates the direction and imitates the relative magnitude of their angular velocities.

By analyzing the responses for a single oscillation as illustrated in fig. 12 it is possible to deduce what cases the oscillations. Figure 13 seeks to increase the comprehensiveness of the impact situation between the spool and sleeve.

The numerated intervals in fig. 12 and 13 are elaborated and correspond to the following:

1. The orifice A_{1314} is closed and the negative angular velocity of the spool is higher than for the sleeve, which indicates that the spool pulls the sleeve along in the counterclockwise direction.

2. The orifice A_{1314} begins to open and $\dot{\theta}_{SL}$ slows down which increases α. A_{1314} opens rapidly due to the orifice is a function α. $\dot{\theta}_{SL}$ changes direction, which causes an impact situation between spool and sleeve when reaching the maximum spring compression at $\alpha = 15°$.

3. As a result of the impact, the spool and sleeve travel as one single body subsequently to the impact.

As the inertia of the spool is considerably larger than that of the sleeve the angular velocity takes longer to decrease than for the sleeve. After a single oscillation, the system returns to its original state until A_{1314} opens again and the dynamics repeat themselves. This happens until the applied input torque at the steering wheel is big enough to counteract that A_{1314} closes.

5.3 Sensitivity Analysis

To illustrate the influence each of the different parameters has on the response, a sensitivity analysis is presented in the following. This analysis is performed to better understand which concepts should be further investigated. Based on an initial parameter variation, the parameters of interest are found to be Coulomb friction, Opening area of orifice A_{10}, and volume variation of V_{2R}. The system responds differently when loaded and unloaded. Therefore, all parameters are analyzed with an input torque applied as a ramp input of 1 Nm/s increased to 6 Nm in the counterclockwise direction and unloaded back to 0 Nm. The sensitivity study is performed for a single parameter at a time and does not take cross-coupled variations into account.

Varying the Coulomb Friction Coefficient

Based on the simulated responses illustrated in fig. 14, an increase in the Coulomb friction coefficient, τ_C, decreases the amplitude of the oscillations. The response shows, that θ_{SP} settles at different values depending on the value of τ_C, when the relative angle, α reaches -15°. This causes the Coulomb friction to increase the torque required to rotate the sleeve and gear set,θ_{SL}. For τ_C increased by a factor of 100, the oscillations disappear. This is due to the Coulomb friction in the gear set, which then is higher than the torque generated by the pressure difference in the gear set and the applied input torque. This prevents the gear set from rotating. Furthermore, an increase in τ_C reduces the range of input torque, where oscillations are present.

The drawback of introducing a higher Coulomb friction effect is that a higher pressure demand for the gear set will increase which will affect the self-alignment speed of the steering wheel and the energy efficiency.

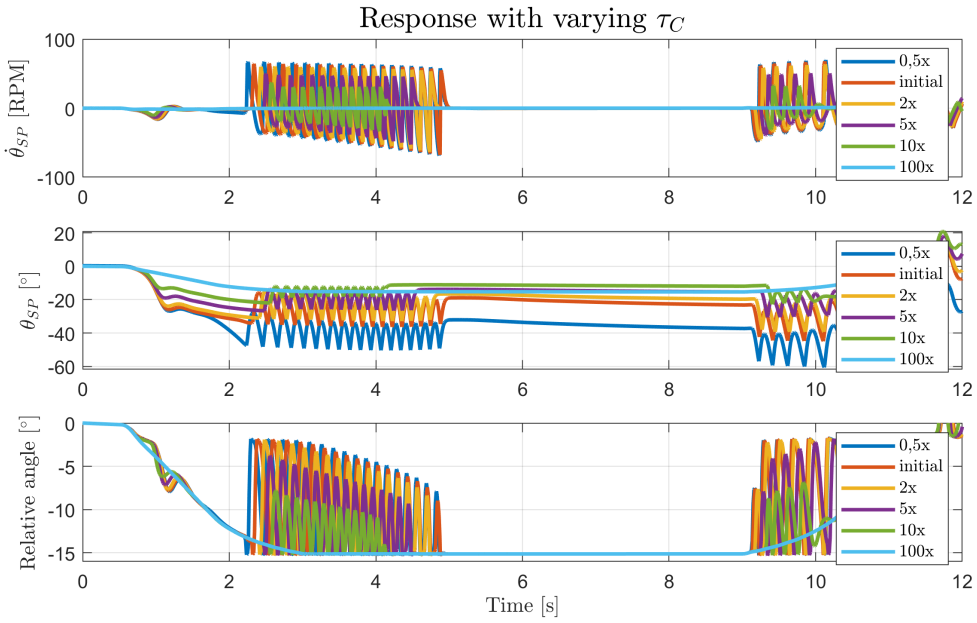

Figure 14: Top: Responses of the steering wheel velocity with varying τ_C, Middle: Responses of the steering wheel position, Bottom: Responses of the relative angle between spool and sleeve.

Varying the Cross-sectional Opening Area of A_{10}

The responses of varying the cross-sectional area A_{10} between a factor of 0.5 to 100 of the initial value is illustrated in fig. 15. A change in the cross-sectional area of A_{10} has a significant influence on the oscillations in $\dot{\theta}_{SP}$. An increase of two times A_{10} results in a 50% reduction in the amplitude of the oscillations for the response $\dot{\theta}_{SP}$. With five times the initial value of A_{10} the oscillations disappear entirely. The torque input resulting in oscillations is also affected by the size of A_{10}, as the oscillations disappear at τ_{ext} = 4 Nm with two times the area, and τ_{ext} = 5 Nm at the initial value. However, it has no influence on the required torque for the oscillations to start occurring.

The reason for A_{10} to have an effect on the oscillations is that, when the cross-section area of A_{10} is increased, then the pressure in P_2 is lowered. Hence, the pressure difference over the gear set decreases and thereby reducing the oscillations. The prevalence of A_{10} ensures a back pressure on the gear set when turning left and provides the end-stop feeling for the operator. With an increase of the correctional area of 5 times or above, the end stop feeling disappear as the reduction in back pressure in the gear set disappear.

Based on the above, it is difficult to find a compromise of having a A_{10} which results in a high end-stop torque and at the same time doesn't affect the available steering pressure level by a high degree.

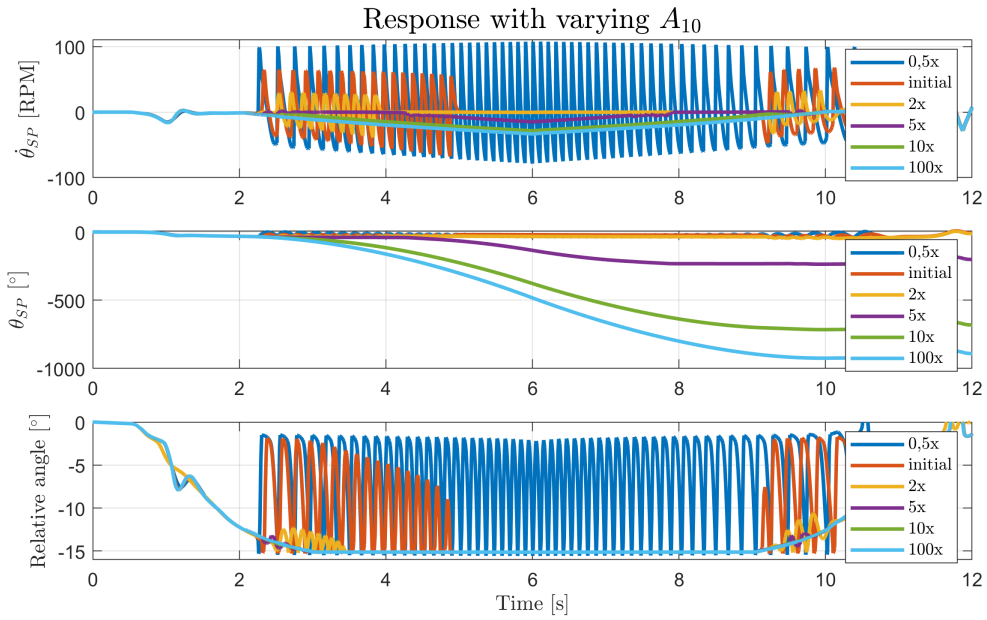

Figure 15: Top: Responses of the steering wheel velocity with varying A_{10}, Middle: Responses of the steering wheel position, Bottom: Responses of the relative angle between spool and sleeve.

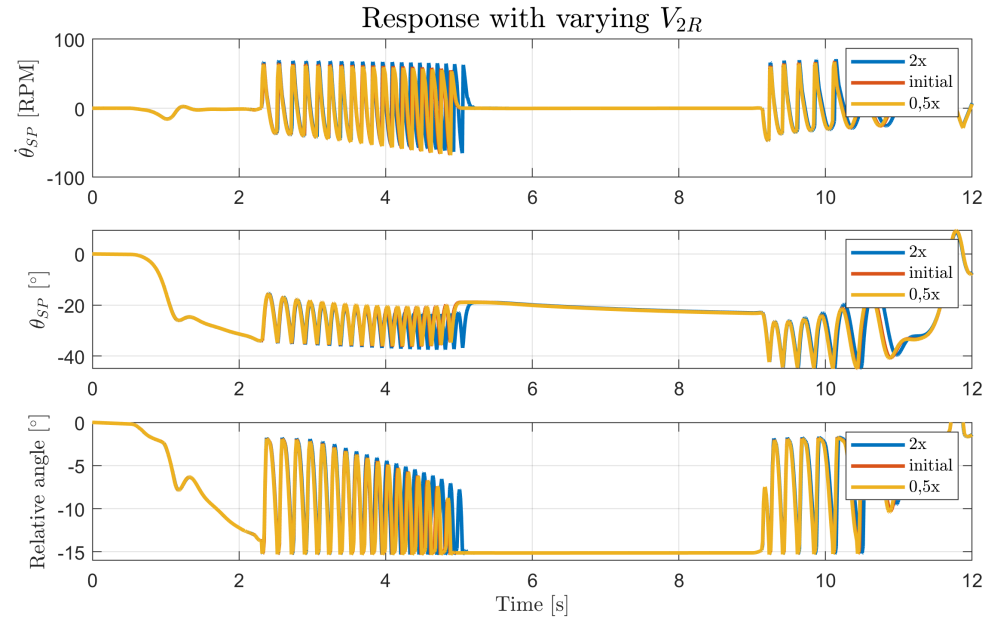

Figure 16: Top: Responses of the steering wheel velocity with varying V_{2R}, Middle: Responses of the steering wheel position, Bottom: Responses of the relative angle between spool and sleeve.

Varying the control volume V_{2R}

The response of varying control volume V_{2R} from the initial design to a factor of two is illustrated in figure 16. From these graphs, it can be seen that the oscillations aren't affected. This observation is further validated by figure 17.

In fig. 17 (c) a comparison of $\dot{P}_{2R}$ is conducted. The initial V_{2R} has a significantly larger pressure gradient than V_{2R} scaled by five. Scaling of V_{2R} has no significant improvement on the oscillations though and the reason can be found in the flow responses during the oscillation, presented in fig. 17 (a). The flow responses in V_{2R} show that the flow in and out of V_{2R} is approximately equal to each other. When V_{2R} is increased by a factor of five, the flow responses are slower, which affects P_{2R}. A_{3R} is dependent on α and the opening area reduces when α approach zero. At 2.99 s in fig. 17, P_{2R} increases due to more flow entering the control volume than leaving. α obtains a larger amplitude, which has an amplifying effect. This combination of events causes V_{2R} to have an insignificant effect on reducing the oscillations.

Looking at the continuity equation it was assumed that the effect which P_{2R} has on τ_{GS}, would reduce the oscillations when V_{2R} was increased. This indicates that sometimes cross-coupled effects can not be ignored, which is the case with the volume here.

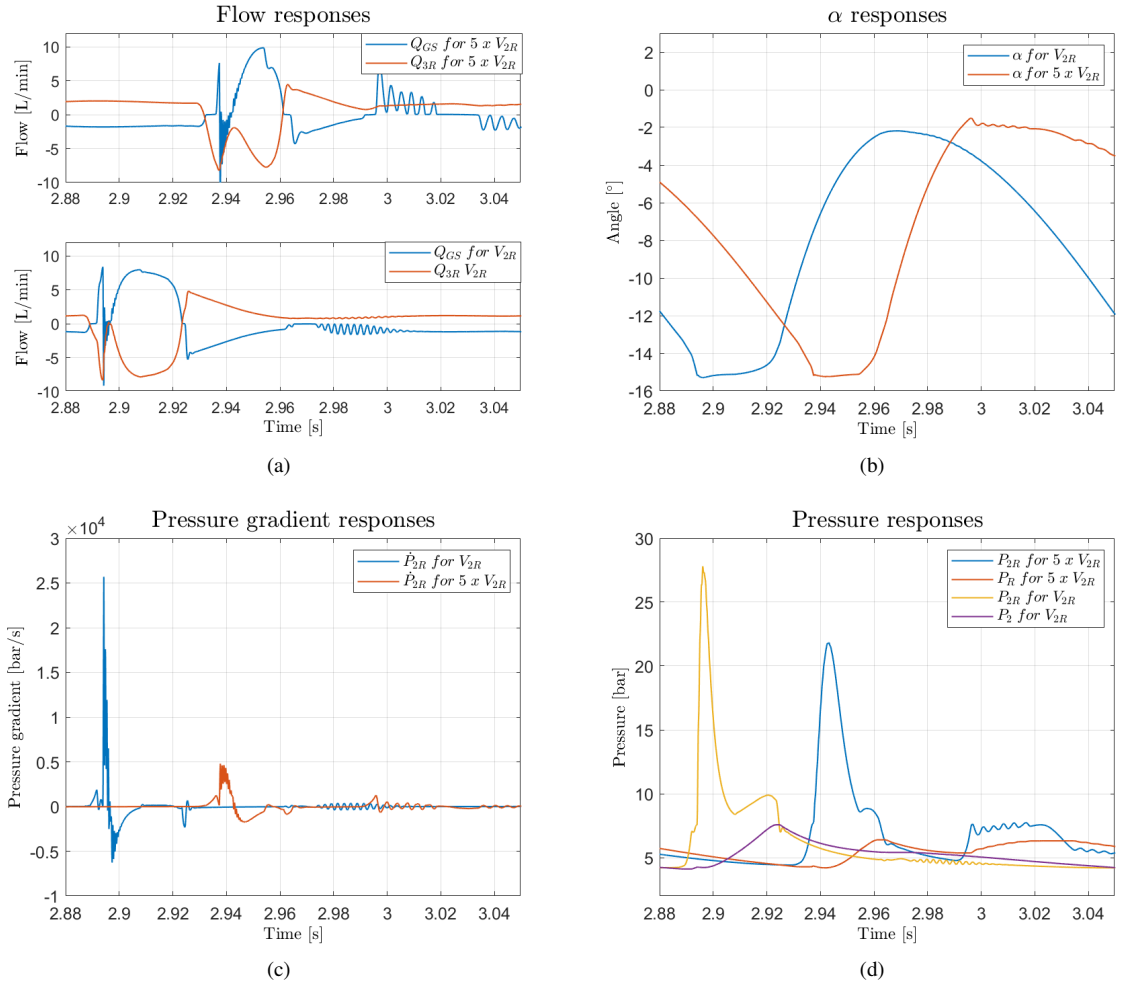

Figure 17: These graphs illustrate the time span for the last oscillation for $5xV_R$ before A_{1314} fully opens.

6 Conclusion

The objective of the paper was to analyze the end-stop oscillations on the new asymmetric ssteer concept, where steering wheel oscillations arise when reaching the left end stroke position. The challenge is to increase the left-side end stroke torque, to ensure that the operator knows that the end-stop is reached, without introducing underdamped oscillations of the steering wheel.

It can here be concluded that a lumped parameter model, of the steering unit in end stop situation, is able to simulate the same behavior as seen in reality. A interesting point is here that the oscillations felt at the left endstroke depends on a given input torque range, which fits very well with the reality.

It can be concluded that the lumped parameters are verified from experimental laboratory test at Danfoss Power Solution. Where matching flow, pressure and velocity profiles where taking into account. The verified model is able to describe how, why, and when the underdamped oscillations are introduced in the system response.

Finally, it can be concluded that a sensitivity study has been performed with the outcome that the coulumb friction coefficient τ_C and the return bleed A_{10} has a significant influence on the underdamped oscillations introduced at the left end stop. This matches with experimental test from Danfoss Power Solution, stating that higher friction is decreasing and completely eliminating the oscillations.

The findings of the study has impacted the end stop concepts at Danfoss Power Solution, such that a new concept is developed without the drawback of underdamped oscillations.

References

[1] GOV. UK. Tractors and regulatory requirements: a brief guide, 9 2017.

[2] J. Tornros and A. Bolling. Mobile phone use - effects of conversation on mental workload and driving speed in rural and urban environments. *Pergamon*, pages 298–306, 2006.

[3] S. et. al. De Craen. The development of a method to measure speed adaptation to traffic complexity: Identifying novice, unsafe, and overconfident drivers. *Pergamon*, pages 1524–1530, 2008.

[4] Heissing B. and Ersoy M. *Chassis handbook: fundamentals, driving dynamics, components, mechatronics, perspectives*. Vieweg + Teubner, 2011.

[5] Danfoss Power Solutions. *OSPB/C/F/D/L LS, OLS Priority Valves, OSQ Flow Amplifiers*, 2019.

[6] Danfoss Power Solutions. Steer-by-wire solutions, 11 2022.

[7] Nuksit Noomwongs and Sunhapos Chantranuwathana. Evaluation of deadband effect in steer-by-wire force feedback system by using driving simulator. *Scientific.Net*, pages 288–291, 8 2014.

[8] Emil N. Olesen and Torben Ole Andersen. Investigation of a new orbital steering concept with focus on the control loop performance. *ASME*, pages 1–7, 9 2022.

[9] August Brandi Mogens Frederiksen Thomas H. Langer Afshin Samani Peter Dam, Malthe Bilgram. Evaluation of two different steering units, in terms of self-alignmenet and deadband, on mental workload during driving of agricultural tractors. pages 1–14, 2019.

[10] Anders Hedegaard Hansen. Fluid power systems, 2019.

[11] Emil NÃ¸rregÃ¥rd Olesen. Development engineer - danfoss power solutions aps, 2022.

[12] Emil NÃ¸rregÃ¥rd Olesen. *A case study investigation of an engineering department at Danfoss with focus on the handling of the digitalization*. Aau, 1st edition, 2020.

[13] Mohieddine Jelali and Andreas Kroll. *Hydraulic Servo-systems Modelling,Identification and Control*. 2003.